

Micro-Raman study on the softening and stiffening of phonons in rutile titanium dioxide film: Competing effects of structural defects, crystallite size, and lattice strain

Subodh K. Gautam, Fouran Singh, I. Sulania, R. G. Singh, P. K. Kulriya, and E. Pippel

Citation: [Journal of Applied Physics](#) **115**, 143504 (2014); doi: 10.1063/1.4868079

View online: <http://dx.doi.org/10.1063/1.4868079>

View Table of Contents: <http://scitation.aip.org/content/aip/journal/jap/115/14?ver=pdfcov>

Published by the [AIP Publishing](#)

Articles you may be interested in

[Softening of phonons by lattice defects and structural strain in heavy ion irradiated nanocrystalline zinc oxide films](#)

J. Appl. Phys. **110**, 083520 (2011); 10.1063/1.3651638

[Size effect on the lattice parameters of nanocrystalline anatase](#)

Appl. Phys. Lett. **95**, 191906 (2009); 10.1063/1.3261754

[Anisotropic biaxial stresses in diamond films by polarized Raman spectroscopy of cubic polycrystals](#)

J. Appl. Phys. **104**, 023524 (2008); 10.1063/1.2959338

[Approach to interface roughness of silicide thin films by micro-Raman imaging](#)

J. Vac. Sci. Technol. B **23**, 468 (2005); 10.1116/1.1868646

[Influence of crystallite size distribution on the micro-Raman analysis of porous Si](#)

Appl. Phys. Lett. **78**, 715 (2001); 10.1063/1.1343494

High-Voltage Amplifiers

- Voltage Range from $\pm 50V$ to $\pm 60kV$
- Current to 25A

Electrostatic Voltmeters

- Contacting & Non-contacting
- Sensitive to 1mV
- Measure to 20kV



ENABLING RESEARCH AND INNOVATION IN DIELECTRICS, ELECTROSTATICS, MATERIALS, PLASMAS AND PIEZOS



www.trekinc.com

TREK, INC. 190 Walnut Street, Lockport, NY 14094 USA • Toll Free in USA 1-800-FOR-TREK • (t):716-438-7555 • (f):716-201-1804 • sales@trekinc.com

Micro-Raman study on the softening and stiffening of phonons in rutile titanium dioxide film: Competing effects of structural defects, crystallite size, and lattice strain

Subodh K. Gautam,¹ Fouran Singh,^{1,a)} I. Sulania,¹ R. G. Singh,² P. K. Kulriya,¹ and E. Pippel³

¹Materials Science Group, Inter University Accelerator Centre, Aruna Asaf Ali Marg, New Delhi 110067, India

²Department of Physics, Bhagini Nivedita College, Delhi University, Delhi 110043, India

³Max Planck Institute of Microstructure Physics, Weinberg 2, D-06120 Halle, Germany

(Received 23 December 2013; accepted 27 February 2014; published online 9 April 2014)

Softening and stiffening of phonons in rutile titanium dioxide films are investigated by *in situ* micro-Raman studies during energetic ion irradiation. The *in situ* study minimized other possible mechanisms of phonon dynamics. Initial softening and broadening of Raman shift are attributed to the phonon confinement by structural defects and loss of stoichiometry. The stiffening of A_{1g} mode is ascribed to large distortion of TiO_6 octahedra under the influence of lattice strain in the (110) plane, which gives rise to lengthening of equatorial Ti-O bond and shortening of apical Ti-O bond. The shortening of apical Ti-O bond induces stiffening of A_{1g} mode in the framework of the bond-order-length-strength correlation mechanism. © 2014 AIP Publishing LLC. [<http://dx.doi.org/10.1063/1.4868079>]

I. INTRODUCTION

The study of transition metal oxides and their nanostructures has great potential for the research activities due to a variety of applications such as transparent conducting window materials for solar cells, electron injecting materials in hybrid and dye sensitized solar cells, chemical sensors, catalysis, water splitting for hydrogen storage, and nanomedicines.^{1–6} Particularly, titanium dioxide (TiO_2) has wide interest in fundamental understanding of phase transition and the response of their physio-chemical properties due to changes in the crystallite size and stoichiometry. It is also very susceptible to change in lattice parameters, which affects the whole lattice dynamics of the materials. Therefore, the study of phonon structure and their dispersion is essential to develop any device based on TiO_2 . In view of such implications, the origin of Raman shift is a topic of discussion, as most of the theoretical calculations are based on a continuum dielectric mechanism. Most of these calculations have been carried out using correlation length, bulk phonon dispersion, and lattice dynamics matrix in accordance with microscopic valence force field, phonon confinement, and bond polarization model. There are reports that the reduction in size leads to the modifications in phonon dispersion and can be understood by the phonon confinement model (PCM).^{7–11} But, PCM is a phenomenological model and does not take into account many parameters such as structural or chemical defects and particle-medium interaction; hence it fails to explain the phonon response for the size of nanoparticles below 10–15 nm.^{11–14} As a matter of fact, size dependent Raman shift has also been attributed to surface disorder, structural stress, bond order length strength

(BOLS) correlation mechanism, and local bond averaging model.^{15–19} However, the softening of phonons has been successfully explained using various mechanisms, but rather limited literature is available about the stiffening of phonons and their possible mechanism.²⁰ Moreover, these models have been demonstrated in different type of materials such as powders, thin films, and prepared in various environments. Therefore, some *in situ* study on single sample would be more appropriate to have better understanding of phonon dynamics and their possible mechanism responsible for such phonon interaction processes.

The rutile tetragonal crystalline structure of TiO_2 exhibits 18 vibrational modes in the first Brillouin zone.¹² Among these 18 modes, only 4 are Raman active: three non-degenerate modes A_{1g} , B_{1g} , B_{2g} , and a doubly degenerate E_g mode. In all Raman active modes, oxygen atom vibrates and Ti remains at rest. The non-degenerate A_{1g} , B_{1g} , and B_{2g} vibrates in the plane perpendicular to *c*-axis, while the doubly degenerate E_g mode vibrates along *c*-axis. The B_{1g} mode consists of rotation of oxygen atom around *c*-axis, with all six oxygen atoms of octahedra that participate in the vibrations. However, the Raman study of such low dimensional TiO_2 films is necessary, as the excess energy at the surface not only controls the elastic properties²¹ but also many other important and relevant properties such as band gap enhancement, core level shifting, and the increase of electron affinity. Moreover, the ultimate effect of the decrease in bond number and bond strengthening as compared to their bulk value dictates the surface chemistry such as wettability, diffusivity, and reactivity. It also affects the thermal/structural stability such as melting, evaporation, and self assembly growth.

It is well known that energetic ion irradiation induced defects in such oxide semiconductors can gives rise to interesting properties such as phase transitions,^{22–24} Fermi level modification,²⁵ d^0 magnetization,²⁶ and even provides scope

^{a)}Author to whom correspondence should be addressed. Electronic mail: fouran@gmail.com. Telephone: +91-11-26893955. Fax: +91-11-26893666.

of understanding of the phonon evolution in oxide semiconductors.²⁷ Therefore, in the present manuscript, the density of structural defects and lattice strain induced by energetic ions and origin or validity of various models as discussed above have been selectively tested by minimizing other possible mechanisms as reported in the literature.

II. EXPERIMENTAL DETAILS

For the present study, ion beam sputtered films on silicon with silica as buffer layer are used. As-deposited films contain mixed anatase and rutile phase with tetragonal structure. Therefore, films were annealed at 1050 °C for 1 h in controlled oxygen environment to have complete phase transition to rutile phase. The temperature of complete phase transition is selected on the basis of a series of annealing studies performed at different temperatures. One such film is used for *in situ* micro-Raman spectroscopy (m-RS) during energetic ion beam irradiation using Renishaw InVia Raman microscope equipped with a fiber optic probe (FOP). After each increment in ion fluence, the target ladder is rotated by 90° for recording the micro-Raman spectra and detail of this facility will be published elsewhere. Another similar film is used for *in situ* grazing incidence x-ray diffraction (GIXRD) using a Bruker D8 advanced diffractometer equipped with copper anode as described elsewhere.²⁸ Selected cross sectional high resolution transmission electron microscopy (X-HRTEM) is also carried out using FEI TITAN 80–300 electron microscopy facility at MPI, Halle. For irradiation, 120 MeV Ag ions were used, which deposits 20.61 keV/nm and 0.085 keV/nm in electronic and atomic sub-systems, respectively, as estimated using SRIM2013 code.²⁹ Therefore, the energy deposited in electronic sub systems is mainly responsible for creating large density of defects and structural strain in the lattice. However, the contribution of the energy deposited in atomic sub-systems cannot be ignored completely. All the experiments were carried out at room temperature.

III. RESULTS AND DISCUSSION

Fig. 1(a) shows m-RS spectra recorded *in situ* during the irradiation at incremented ion fluences up to 2×10^{13} ions/cm², while Figs. 1(b) and 1(c) show the peak shape analysis in terms of Raman shift and the corresponding full width at half maxima (FWHM) of E_g and A_{1g} phonon modes, respectively. It is noted that the pristine film shows all the four Raman active modes such as B_{1g} , E_g , A_{1g} , and B_{2g} at 143, 443, 609, and 826 cm⁻¹, respectively. This spectrum also shows a second order band of Raman shift around 230 cm⁻¹. The observation of these modes reveals that those films are highly crystalline with rutile tetragonal structure. It is also seen from the spectra that the intensity of the peaks monotonously decreases with increasing ion fluences of energetic ions. E_g mode shows a softening up to the fluence of 4×10^{12} ions/cm² and followed by some stiffening, if fluence is further increased; while the FWHM shows a continuous increase with increase in ion fluence. Few representatives Lorentzian fitted Raman spectra are submitted as supplementary material.³⁰ It may also be noted that the response of this mode at

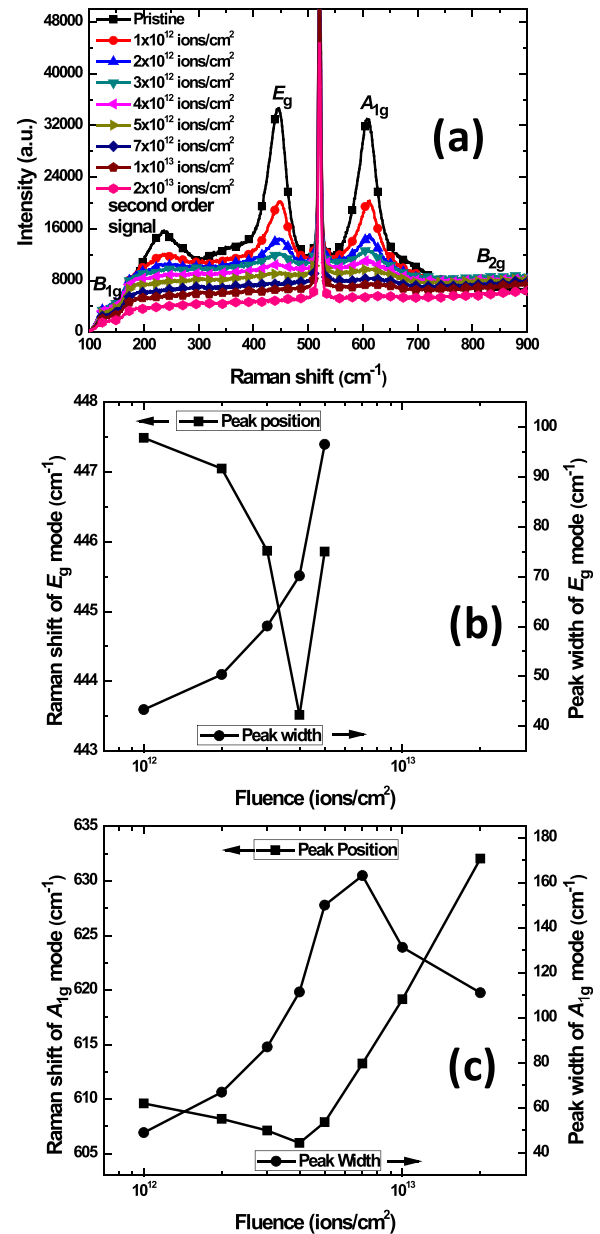


FIG. 1. (a) Micro-Raman spectra recorded *in situ* during energetic ion irradiation at various ion fluences, (b) peak shape analysis of E_g mode, and (c) peak shape analysis of A_{1g} mode of rutile TiO_2 films.

higher fluences could not be reported, as this mode completely disappears at a fluence of 5×10^{12} ions/cm². On the other hand, A_{1g} mode also shows a softening up to the fluence of 4×10^{12} ions/cm², followed by stiffening at higher fluences up to 2×10^{13} ions/cm². However, the FWHM of this mode shows a monotonous increase only up to a fluence of 7×10^{12} ions/cm², followed by a decrease at higher fluences.

Fig. 2(a) shows GIXRD pattern of the pristine film with the diffraction peaks of (110), (101), (200), (111), and (210) planes of the rutile phase of TiO_2 , with crystal structure $P4_2/mnm$ (JCPDS Card No. 21-1276). The lattice parameters, as calculated using Powderx software, are found to be $a = 4.593 \text{ \AA}$ and $c = 2.953 \text{ \AA}$. The observed values are very close to the lattice parameters of bulk rutile TiO_2 . It is also clear from the pattern that the film is polycrystalline in

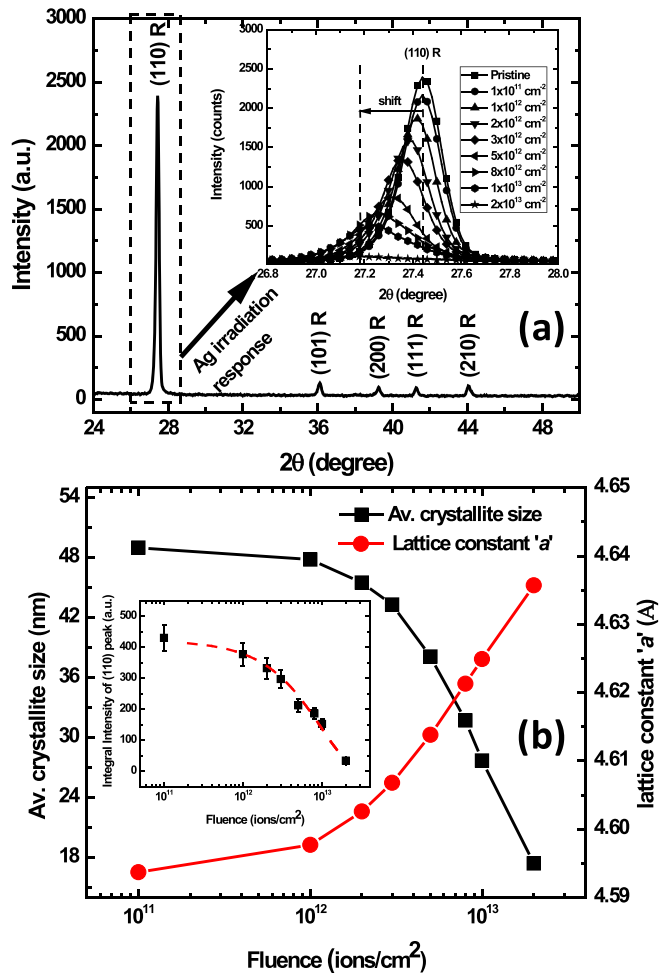


FIG. 2. (a) GIXRD pattern of rutile TiO_2 film, while inset of the same figure shows the response of (110) diffraction peak under 120 MeV Ag ion irradiation recorded *in situ* during energetic ion irradiation. (b) average crystallite size and lattice constant “ a ” calculated from the GIXRD pattern, while inset shows the decrease in the integral peak intensity of (110) diffraction and a fit using Gibbon’s formula for calculating the cross section of amorphization.

nature. The inset of the figure shows the response of 120 MeV Ag ions on (110) plane recorded *in situ* during irradiation at incremented ion fluences. Average crystallite size is calculated using Scherer’s formula by using the FWHM of (110) diffraction peak corrected for the instrumental broadening and are shown on left axis of Fig. 2(b). The structural analysis for determining the lattice parameters is carried out using Powderx and observed an expansion in the (110) plane as evidenced by increase in the lattice parameter “ a ” with an increase in ion fluences and is shown on the right axis of Fig. 2(b). The calculated value of the lattice parameter “ a ” for the highest fluences is to be 4.635 Å. The micro-structural strain is also evaluated using the variation in the lattice parameters and will be discussed in the ninth paragraph of this manuscript. This analysis reveals that the mean size of crystallites decreases, while the lattice parameter “ a ” increases in the (110) plane with increasing ion fluences.

Inset of Fig. 2(b) shows the variation in the integral intensity of the diffraction peak from (110) plane with increasing ion fluence by symbols. It can be clearly seen that the crystalline fraction decreases and the amorphous

fraction increases with increasing ion fluence. The cross section of amorphization can be calculated using Gibbon’s formula³¹

$$A = A_0 e^{-a\Phi},$$

where A is the crystalline fraction, which decreases with increase in ion fluence, and A_0 is the total crystalline fraction. While, $a = \pi r^2$ is the cross section of amorphization, where r is the radius of ion track and Φ is the ion fluence. The size of ion tracks is estimated by fitting this equation and is found to be 1.81 ± 0.16 nm. The calculated value is quite consistent with the value reported in literature.^{32,33}

The effect of energetic ion induced changes in microstructure, crystallite size, and amorphization is further investigated using the cross sectional high resolution transmission electron microscopy (X-HRTEM) as shown in Fig. 3. Images of Figs. 3(a) and 3(b) clearly reveal that pristine films are highly crystalline in nature, which are consistent with the XRD results. However, the film irradiated for the highest fluence shows that the film is amorphized with some crystalline nanoparticles as shown in Figs. 3(c) and 3(d). Moreover, the density in such nanoparticles is very small and their size varies from 4 to 10 nm. These nanoparticles are surrounded by amorphous TiO_2 , which enormously affects the phonon structure and will be discussed in the following section.

This study has shown the way for an in-depth understanding of the softening and stiffening of phonons. As a matter of fact, position of Raman shift and FWHM of the same are also plotted as function of crystallite size using the data of *in situ* m-RS and GIXRD and are shown in Fig. 4. The inset of the same figure shows the evolution of strain in (110) surface of rutile TiO_2 as a function of crystallite size. Results show that as the size decreases from 50 to 40 nm, A_{1g} mode shows softening of about 3 cm^{-1} along with increase

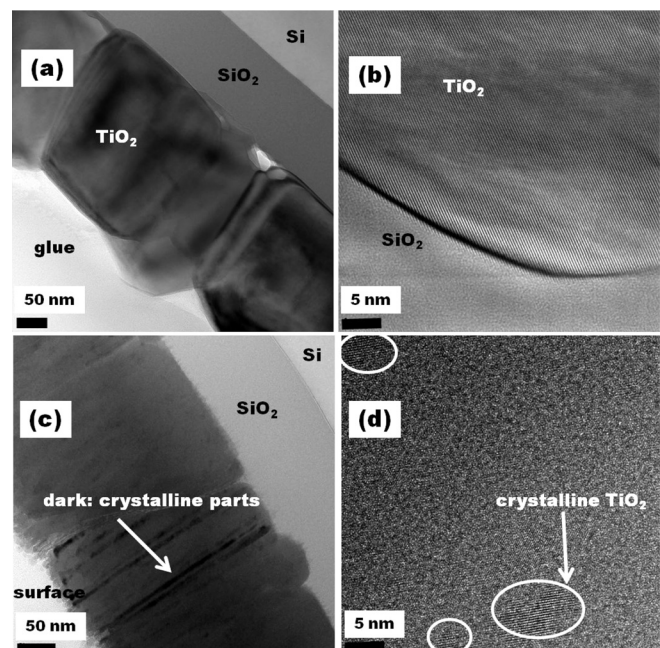


FIG. 3. Cross section HRTEM images of (a) and (b) pristine; and (c) and (d) film irradiated with a fluence of 2×10^{13} ions/cm² using 120 MeV Ag ions.

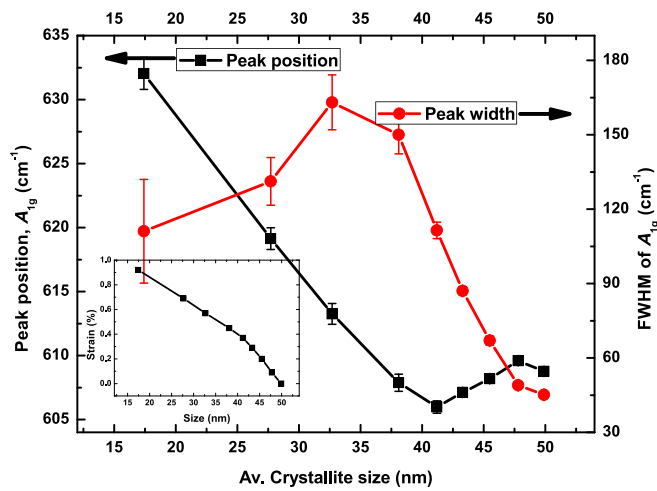


FIG. 4. Variation in peak position and peak width of A_{1g} mode with changes in average crystallite size as calculated from GIXRD study. Inset shows the evolution of strain in (110) surface with variation in average crystallite size. Origin of the stress is attributed to the density of oxygen vacancies induced by energetic ion irradiation.

in peak width. However, a further decrease in the size leads to the stiffening of this mode even up to the size of about 15 nm. However, the FWHM of the peak increases only up to a size of about 30 nm, followed by decrease on further reduction in size of crystallites. It would be pertinent to mention that even the E_g mode shows a similar response up to the size of about 42 nm. But, the response of this E_g mode cannot be investigated at smaller sizes, as it completely disappears below this. Therefore, the following discussion is based on the response of A_{1g} mode only.

According to the PCM, each mode should exhibit red shifting in peak position with asymmetric peak broadening. There are many mechanisms of PCM that explains softening,

for instance, phonon confinement by reduction in size,^{7–11} surface stress,^{34–36} and structural defects.²⁷ The softening can also be understood by the loss of stoichiometry^{37,38} and local heating effects.³⁹ However, in the present study, the effect of reduction in size is not possible because the size of the crystallites in the region of softening is bigger than 30 nm, and E_g mode also shows softening (which is supposed to show stiffening with decrease in size). The effect of local heating is also unlikely, as all the measurements were carried out at same temperature with same laser power for excitation. Therefore, the initial softening of A_{1g} phonons of $\sim 3 \text{ cm}^{-1}$ can be attributed to the phonon confinement by lattice defects such density of oxygen vacancies, which gives rise structural strain and loss of stoichiometry.^{24,27} The evolution of strain in (110) surface induced by oxygen vacancies is in agreement with the reported prediction of first principle calculations.⁴⁰ In very recent work, the same group has also shown that this kind of strain engineering can be used to tailor the elastic properties and reactivity of the surfaces.²¹ For the evidence of loss of stoichiometry in irradiated film, the loss of oxygen is confirmed by the cross sectional line scan of energy dispersive x-ray (EDX) analysis as shown in Fig. 5. EDX scan clearly shows that there is almost no change in the concentration of Ti along the thickness of the film, while oxygen depletion is evident from the film.

There are rather limited studies which are reported on the stiffening of A_{1g} modes of rutile TiO_2 and their possible mechanisms.²⁰ The observed stiffening of A_{1g} mode as evidenced by the blue shifting of this mode below the size of about 30 nm is ascribed to BOLS correlation mechanism.^{15–19} According to this mechanism, the lattice periodicity is terminated with reduction in size and leads to the contraction of bonds between the surface atoms. For instance, if d is the normal bond length and it can be contracted to d_i , under the

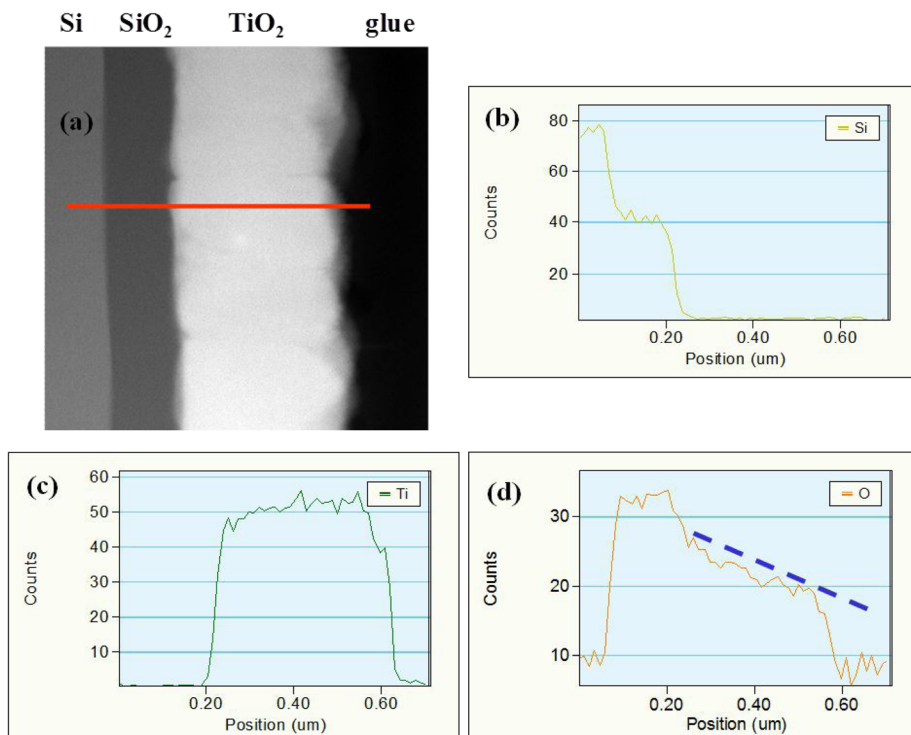


FIG. 5. Cross sectional EDX line scan for Si, Ti, and O from the film irradiated with fluence of 2×10^{13} ions/cm² using 120 MeV Ag ions.

terminations of periodicity, then the contracted bond length, $d_i = c_i d$, where c_i is the coefficient of bond contraction. Thus, there will be an increase in the bond strength, which can be derived as, $E_i = c_i^{-m} E_b$, where m is the index of bond nature. The experimental results of present study demonstrate that the high density of oxygen vacancies in (110) surface induced tensile strain, which leads to increase in the equatorial Ti-O bond length and shortening of apical Ti-O bond. Thus, the apical bond is strengthened and gives rise to the stiffening of A_{1g} modes as described in Ref. 20 and reasonably well evidenced by the BOLS correlation mechanism.

IV. CONCLUSIONS

In summary, *in situ* micro-Raman investigations provide the scope for the understanding of the phonon dynamics in rutile TiO₂. The initial softening of the phonons is attributed to the phonon confinement by lattice defects such as density of oxygen vacancies and loss of stoichiometry. The interplay between density of oxygen vacancies and strain in (110) surface is also demonstrated in agreement with the prediction of the comprehensive first principle calculations. The controlled stiffening of A_{1g} phonons is experimentally observed and ascribed to bond strengthening of apical Ti-O bond under large distortion of TiO₆ octahedra induced by lattice strain in the (110) plane within the frame work of BOLS correlation mechanism. Therefore, such studies could be useful for many functionalities such as sensors, origin of d^0 magnetization of dilute magnetic semiconducting materials, catalysis, and other surface related properties. Finally, it can be concluded that energetic ions can be used efficiently for an in-depth understanding of the origin and dynamics of the phonon interactions.

ACKNOWLEDGMENTS

Authors are grateful to Dr. A. Tripathi, Dr. D. K. Avasthi, and Dr. D. Kanjilal (Director, IUAC) for their constant encouragement. Authors are also grateful to Dr. A. Roy (Former Director, IUAC) for extending all kinds of moral and financial supports for the implementation of *in situ* micro-Raman facility including beamtime allotment in Director discretionary quota (DDQ) for the testing the facility. Authors take this opportunity to extend their special thank to Dr. J. C. Pivin for sparing time for fruitful discussions and Dr. C. P. Safvan for improving the English of the manuscript. Pelletron group is also acknowledged for providing the stable beam during ion irradiation experiment. The multi-tasking support for the realization of *in situ* micro-Raman facility from workshop, vacuum lab and application/service engineers of Renishaw UK is highly acknowledged. Department of Science and Technology (DST), Government of India is acknowledged for providing the XRD facility to IUAC under the IRPHA project. One of the authors (S.K.G.) acknowledges Senior Research Fellowship (SRF) Grant No. [09/760(0024)/2011-EMR-I] from Council for Scientific and Industrial Research (CSIR); while F.S. is grateful to DST,

Government of India for providing Science and Engineering Research Board (SERB) Project (SB/EMEQ-122/2013).

- ¹A. Fujishima and K. Honda, *Nature (London)* **238**, 37 (1972).
- ²A. Mills and S. Le Hunte, *J. Photochem. Photobiol., A* **108**, 1 (1997).
- ³H. Liu, H. T. Ma, X. Z. Li, W. Z. Li, M. Wu, and X. H. Bao, *Chemosphere* **50**, 39 (2003).
- ⁴R. K. Karn and O. N. Srivastava, *Int. J. Hydrogen Energy* **24**, 27 (1999).
- ⁵A. M. G. Kang, N.-G. Park, Y. J. Park, K. S. Ryu, and S. H. Chang, *Sol. Energy Mater. Sol. Cells* **75**, 475 (2003).
- ⁶A. P. Singh, S. Kumari, A. Tripathi, F. Singh, K. J. Gaskell, R. Shrivastav, S. Dass, S. H. Ehrman, and V. R. Satsangi, *J. Phys. Chem. C* **114**, 622 (2010).
- ⁷T. Mazza, E. Barborini, P. Piseri, P. Milani, D. Cattaneo, A. Li Bassi, C. E. Bottani, and C. Ducati, *Phys. Rev. B* **75**, 045416 (2007).
- ⁸V. Swamy, B. C. Muddle, and Q. Dai, *Appl. Phys. Lett.* **89**, 163118 (2006).
- ⁹V. Swamy, *Phys. Rev. B* **77**, 195414 (2008).
- ¹⁰T. Mazza and P. Milani, *Appl. Phys. Lett.* **91**, 046103 (2007).
- ¹¹L. Bassi, D. Cattaneo, V. Russo, C. E. Bottani, E. Barborini, T. Mazza, P. Piseri, P. Milani, F. O. Ernst, K. Wegner, and S. E. Pratsinis, *J. Appl. Phys.* **98**, 074305 (2005).
- ¹²A. Dieguez, A. Romano-Rodriguez, A. Vila, and J. R. Morante, *J. Appl. Phys.* **90**, 1550 (2001).
- ¹³H. Richter, Z. P. Wang, and L. Ley, *Solid State Commun.* **39**, 625 (1981).
- ¹⁴I. H. Campbell and P. M. Fauchet, *Solid State Commun.* **58**, 739 (1986).
- ¹⁵Q. Sun, *Prog. Solid State Chem.* **35**, 1 (2007).
- ¹⁶Q. Sun, *Prog. Mater. Sci.* **54**, 179 (2009).
- ¹⁷L. K. Pan, C. Q. Sun, and C. M. Li, *J. Phys. Chem. B* **108**, L3404 (2004).
- ¹⁸Q. Sun, Y. Shi, C. M. Li, S. Li, and T. C. Au Yeung, *Phys. Rev. B* **73**, 075408 (2006).
- ¹⁹X. J. Liu, L. K. Pan, Z. Sun, Y. M. Chen, X. X. Yang, L. W. Yang, Z. F. Zhou, and C. Q. Sun, *J. Appl. Phys.* **110**, 044322 (2011).
- ²⁰R. Aita, *Appl. Phys. Lett.* **90**, 213112 (2007).
- ²¹L. Jia, D.-J. Shu, and M. Wang, *Phys. Rev. Lett.* **109**, 156104 (2012).
- ²²H. Rath, P. Dash, T. Som, P. V. Satyam, U. P. Singh, P. K. Kulriya, D. Kanjilal, D. K. Avasthi, and N. C. Mishra, *J. Appl. Phys.* **105**, 074311 (2009).
- ²³A. Benyagoub, F. Levesque, F. Couvreur, C. Gibert-Mougel, C. Dufour, and E. Paumier, *Appl. Phys. Lett.* **77**, 3197 (2000); *Phys. Rev. B* **72**, 094114 (2005).
- ²⁴F. Singh, B. Chaudhary, V. Kumar, R. G. Singh, S. Kumar, and A. Kapoor, *J. Appl. Phys.* **112**, 073101 (2012).
- ²⁵A. Kumar, M. K. Jaiswal, D. Kanjilal, R. K. Joshi, and T. Mohanty, *Appl. Phys. Lett.* **99**, 013109 (2011).
- ²⁶H. Thakur, R. Kumar, P. Thakur, N. B. Brookes, K. K. Sharma, A. P. Singh, Y. Kumar, S. Gautam, and K. H. Chae, *Appl. Phys. Lett.* **98**, 192512 (2011); *J. Appl. Phys.* **110**, 083718 (2011).
- ²⁷F. Singh, R. G. Singh, V. Kumar, S. A. Khan, and J. C. Pivin, *J. Appl. Phys.* **110**, 083520 (2011); F. Singh, P. K. Kulriya, and J. C. Pivin, *Solid State Commun.* **150**, 1751 (2010).
- ²⁸P. K. Kulriya, F. Singh, A. Tripathi, R. Ahuja, A. Kothari, R. N. Dutt, Y. K. Mishra, A. Kumar, and D. K. Avasthi, *Rev. Sci. Instrum.* **78**, 113901 (2007).
- ²⁹J. F. Ziegler, M. D. Ziegler, and J. P. Biersack, *Nucl. Instrum. Methods B* **268**, 1818 (2010).
- ³⁰See supplementary material as <http://dx.doi.org/10.1063/1.4868079> for representatives Lorentzian fitted Raman spectra.
- ³¹J. F. Gibbons, *Proc. IEEE* **60**, 1062 (1972).
- ³²K. Awazu, X. Wang, M. Fujimaki, T. Komatsubara, T. Ikeda, and Y. Ohki, *J. Appl. Phys.* **100**, 044308 (2006).
- ³³K.-I. Nomura, T. Nakanishi, Y. Nagasawa, Y. Ohki, K. Awazu, M. Fujimaki, N. Kobayashi, S. Ishii, and K. Shima, *Phys. Rev. B* **68**, 064106 (2003).
- ³⁴E. Anastassakis and E. Liarokapis, *J. Appl. Phys.* **62**, 3346 (1987).
- ³⁵V. B. Shenoy, *Phys. Rev. B* **71**, 094104 (2005).
- ³⁶Y. I. Yuzyuk, R. S. Katiyar, V. A. Alyoshin, I. N. Zakharchenko, D. A. Markov, and E. V. Sviridov, *Phys. Rev. B* **68**, 104104 (2003).
- ³⁷J. C. Parker and R. W. Siegel, *Appl. Phys. Lett.* **57**, 943 (1990).
- ³⁸W. F. Zhang, Y. L. He, M. S. Zhang, Z. Yin, and Q. Chen, *J. Phys. D: Appl. Phys.* **33**, 912 (2000).
- ³⁹K. A. Alim, V. A. Fonoberov, M. Shamsa, and A. A. Balandin, *J. Appl. Phys.* **97**, 124313 (2005).
- ⁴⁰D.-J. Shu, S.-T. Ge, M. Wang, and N.-B. Ming, *Phys. Rev. Lett.* **101**, 116102 (2008).